

# Simple fluid approach for the nonlinear excitations in Yukawa fluids

Prince Kumar<sup>1</sup>  and Devendra Sharma<sup>1,2</sup> 

<sup>1</sup>Institute for Plasma Research, Bhat, Gandhinagar 382428, India

<sup>2</sup>Homi Bhabha National Institute, Training School Complex, Anushaktinagar, Mumbai 400094, India

Corresponding author: Prince Kumar, [kumarprincephysics@gmail.com](mailto:kumarprincephysics@gmail.com)

(Received 10 July 2024; revision received 24 February 2025; accepted 25 February 2025)

We present a study on the solitons in strongly coupled Yukawa fluids using a simple fluid model (SFE), supplemented by an appropriate equation of state for the medium. The formulation covers a broad range of coupling ( $\Gamma$ ) and screening ( $\kappa$ ) parameters, showing an agreement with the nonlinear quasilocalized charged approximation and generalized hydrodynamic models in the weak screening regime of the solitons in Yukawa media. The results also show a quantitative agreement with the experimentally measured values of the width and Mach number with the normalized amplitude. It has also been observed that the amplitude and width of the soliton in the weak screening limit increase with  $\Gamma$  up to  $\Gamma \sim 10$ , beyond which they remain independent of  $\Gamma$  values. Molecular dynamics simulations also confirm that the localization begins to emerge beyond  $\Gamma \sim 10$ , showing no significant effects on the characteristics of the solitons in Yukawa media. Therefore, the SFE model is capable of predicting the impact of the onset of the localization on the solitons in Yukawa media. Additionally, the amplitude of the soliton increases while its width decreases with  $\kappa$  values. The SFE model also explores the possibility of forming refractive soliton structures, whose intensity increases with  $\kappa$  values and decreases with  $\Gamma$  values.

**Keywords:** Fluid Equations, Yukawa fluid, Generalized Hydrodynamic model

---

## 1. Introduction

Solitons are stable, localized wave packets that maintain their shape and speed while propagating through a medium. They arise due to a delicate balance between nonlinear and dispersive effects, making them a fascinating subject of study in various fields of physics (Gu, 2013, Arora, Rani & Emadifar, 2022). Solitons can be found in numerous settings, including water waves (Craig *et al.* 2006), optical fibres (Gordon, 1983), carbon nanotubes systems (Chamon, 2000, Kumar *et al.* 2022), charged fluids and even biological systems (Gu, 2013, Arora, Rani & Emadifar, 2022). Dusty plasma offers a unique opportunity to study the characteristics of solitons in charged fluids on very accessible spatiotemporal scale (Shukla, 1983). The interaction of the dust particles can be modelled by Yukawa potential, characterizing with the coupling parameter  $\Gamma = Q^2/aT$  and the screening parameter  $\kappa = a/\lambda_d$ ,

where  $Q$ ,  $T$ ,  $a$  and  $\lambda_d$  are the dust charge, dust temperature, lattice constant and screening length, respectively.

These nonlinear excitations in the strongly coupled regime of the medium are well explored using various theoretical models, such as the generalized hydrodynamic (GH) model (Kaw, 2001, Chakrabarti & Ghosh 2015), the nonlinear quasilocated charged approximation (QLCA) model (Prince Kumar and Devendra Sharma, 2023, Prince Kumar and Devendra Sharma, 2022) and molecular dynamical (MD) simulations (Kumar, Tiwari & Das, 2017, Tiwari *et al.* 2015). These models successfully describe the soliton structures within their respective regimes of applicability. The one-component version of the GH model has been applied to describe how the viscoelasticity of the medium affects the solitons, with the relaxation time  $\tau_m$  and the viscosity  $\eta$  as essential parameters (Sharma, Boruah & Bailung, 2014). This version of the GH model has a limited scope, preventing it from effectively exploring the wide range of the screening regime of the nonlinear excitations in Yukawa media (Kaw, 2001). The nonlinear QLCA model, however, overcomes this barrier by incorporating the explicit localization of the constituent particles in the formulation (Prince Kumar and Devendra Sharma, 2023, Prince Kumar and Devendra Sharma, 2021). The QLCA was developed as a framework to model the dielectric response and the dispersion of collective modes in strongly coupled liquid-phase plasmas, where the coupling parameter ( $\Gamma \gg 1$ ) indicates a highly localized regime. Consequently, this framework is applicable only within the localized domain of systems (Prince Kumar and Devendra Sharma, 2023, Golden & Kalman 2000). Moreover, investigating the influence of the parameter  $\Gamma$  on solitons in dusty plasmas is interesting, given the limited insights provided by experimental results. The purpose of this paper is to present a description of the dust solitons across a wide range of parametric values using a simple fluid model (SFE) and to compare it with existing models, MD simulations and experimental results.

The paper presents a SFE model (Khrapak & Thomas 2015), supplemented by a suitable equation of state, to characterize solitons across a broad range of parameters  $\Gamma$  and  $\kappa$ . We adopt the practical expression of the internal energy and the pressure, applicable across coupling regime, to calculate the compressibility of the Yukawa medium (Khrapak & Thomas 2015). The formulation covers a broad range of parameters  $\Gamma$  and  $\kappa$ , consistent with the weak screening limit of the nonlinear QLCA and GH models in characterizing the solitons in Yukawa media. The results obtained within the framework of the SFE model also exhibit a quantitative agreement with experimentally measured values of the width and Mach number for various values of the normalized amplitude (Sharma, Boruah & Bailung, 2014). Agreement is achieved for lower values of  $\kappa$ , and the characteristics of the solitons are not significantly altered by varying the  $\Gamma$  parameter. It has been observed that the amplitude and width of the soliton in the weak screening limit increases with  $\Gamma$  up to the value  $\Gamma \sim 10$ , beyond this value it remains independent of  $\Gamma$  values. The MD simulations presented in this paper also confirm that the localization starts emerging beyond  $\Gamma \sim 10$  which shows no impact on the solitons in Yukawa media. Therefore, the SFE model can accurately predict the effects of the onset of localization on the nonlinear excitations in Yukawa media. The amplitude and width of the soliton increases and decreases, respectively, with  $\kappa$  values. The SFE model also explores the possibility of forming refractive soliton structures whose intensity increases and decreases with  $\kappa$  and  $\Gamma$  values, respectively.

The SFE model may successfully overcome the limitations of the nonlinear QLCA in the weak coupling regime (Prince Kumar and Devendra Sharma, 2023) and the

one-component version of the GH model (Kaw, 2001) in the strong screening limit of the solitons in Yukawa media. However, it is known that the simplistic fluid treatment is applicable to longer wavelengths or low frequencies and becomes irrelevant in the highly localized regime. The fluid model's limited scope prevents it from accessing relatively shorter collective modes, as its phenomenological equation of state is not applicable in this limit (Khrapak & Thomas 2015). The significant contribution to the formation of the Korteweg-de Vries (KdV) solitons, however, comes from lower spectral modes, which are efficiently captured within the framework of the SFE model. Additionally, the precise practical formulations of thermodynamic quantities enable us to achieve quantitative results and conduct detailed comparisons with outcomes from other approaches. The future scope of the formulation is briefly discussed at the end of the paper.

The structure of the article is as follows. The description of the model equations for the soliton in strongly coupled Yukawa media is presented in § 2. The KdV equation is derived using the fluid equations in § 2.1. The analytical KdV results across coupling regime and their comparison with the existing models are presented in § 3. The comparison with the experimental data, the MD simulation, the nonlinear QLCA model and the GH model are presented in §§ 3.2, 3.3, 3.4 and 3.5, respectively. The simulation on the evolution of the general perturbation is presented in § 3.6. The summary and conclusions of the study are presented in § 4.

**2. Simple fluid equations with an equation of state for Yukawa fluids: the SFE model**

The description of long-wavelength collective excitations in a strongly coupled Yukawa fluid can be obtained using the fluid equations that are supplemented with appropriate modified thermodynamic quantities. The momentum and continuity equation for a charged dust fluid are (Khrapak & Thomas 2015)

$$\frac{\partial \mathbf{u}_d}{\partial t} + (\mathbf{u}_d \cdot \nabla) \mathbf{u}_d = \frac{Q}{m_d} \mathbf{E} - \frac{1}{m_d n_d} \nabla P_d, \tag{2.1}$$

$$\frac{\partial n_d}{\partial t} + \nabla \cdot (n_d \mathbf{u}_d) = 0. \tag{2.2}$$

The adiabatic compressibility of the medium can be related to isothermal compressibility by using expression given as

$$\left( \frac{\partial P}{\partial n_d} \right)_S = \gamma \left( \frac{\partial P}{\partial n_d} \right)_T \tag{2.3}$$

where  $S$  is system entropy and  $\gamma = C_P/C_V$  is the adiabatic index. Using above expression, (2.1) can therefore be written as

$$\frac{\partial \mathbf{u}_d}{\partial t} + (\mathbf{u}_d \cdot \nabla) \mathbf{u}_d = \frac{Q}{m_d} \mathbf{E} - V_{th}^2 \gamma \alpha \frac{\nabla n_d}{n_d}, \tag{2.4}$$

where  $V_{th} = \sqrt{T_d/m_d}$  is the thermal velocity of dust particles,  $T_d$  is the dust-thermal energy,  $Q = -Ze$  is the dust charge, the electric field  $\mathbf{E} = -\nabla\phi$  and  $\alpha = (1/T_d) (\partial P/\partial n_d)_T$  is the isothermal compressibility modulus.

Upon normalization, (2.4) takes the form

$$\frac{\partial \mathbf{u}_d}{\partial t} + (\mathbf{u}_d \cdot \nabla) \mathbf{u}_d = \mu \nabla \phi - \frac{\gamma \alpha}{3\Gamma} \frac{\nabla n_d}{n_d}, \tag{2.5}$$

and the normalized Poisson equation becomes

$$\nabla^2 \phi = \frac{1}{\mu} [n_d + n_e - n_i], \quad (2.6)$$

where  $n_e = \delta_e \exp(\sigma_e \phi)$ , and  $n_i = \delta_i \exp(-\sigma_i \phi)$ . We have the dimensionless parameters  $\mu = Z_d T_d / (m_d a^2 \omega_{pd}^2)$ ,  $\delta_e = n_{e0} / Z_d n_{d0}$ ,  $\delta_i = n_{i0} / Z_d n_{d0}$  and  $\sigma_{i,e} = T_d / T_{i,e}$ . The equilibrium dust density  $n_{d0}$ , the ratio  $T_d/e$ , dust acoustic frequency  $\omega_{pd} = \sqrt{4\pi Q^2 n_{d0} / m_d}$  and mean dust separation  $a = (4\pi n_{d0} / 3)^{-1/3}$  are used as normalizations for the density, potential, time and length, respectively. Equations (2.5)–(2.7) along with the continuity (2.2) constitute a nonlinear model as the convective nonlinearity in the second term and the nonlinear second term in right-hand side of (2.5) are retained. The value of the coefficient  $\gamma\alpha$  is given as (Khrapak & Thomas 2015, Khrapak & Thomas 2015)

$$\gamma\alpha = \alpha + \frac{(p - \Gamma (\partial p / \partial \Gamma))^2}{u - \Gamma ((\partial p / \partial \Gamma))} \quad (2.7)$$

where  $u$ ,  $p$  and  $\alpha$  account for particle–particle correlation and plasma-related effects. The  $u(\Gamma, \kappa)$ ,  $p(\Gamma, \kappa)$  and  $\alpha(\Gamma, \kappa)$ , are the system excess energy, pressure and isothermal compressibility modulus (Khrapak & Thomas 2015). The expressions for these parameters are presented in appendix A. The model equations presented here are first used to drive the KdV equation to study soliton structures in Yukawa media across various coupling regimes. This is followed by the analysis of the results and their validation with experimental data, MD simulation, the GH model and the QLCA model. For simplicity, from now on, let  $\alpha = \frac{\gamma\alpha}{3\Gamma}$ .

### 2.1. Derivation of the KdV equation for a strongly coupled Yukawa fluid

In order to obtain the KdV equation (Davidson, 2012) for this system, we first introduce slow variables  $\zeta$  and  $\tau$ , given by

$$\zeta = \epsilon^{1/2}(x - v_0 t), \quad \tau = \epsilon^{3/2} t, \quad (2.8)$$

where  $\epsilon$  is a smallness parameter measuring the weakness of the perturbation and  $V_0$  represent the phase velocity of the dust acoustic wave (DAW). In terms of  $\zeta$  and  $\tau$  the equations become

$$\epsilon^{3/2} \frac{\partial n_d}{\partial \tau} - V_0 \epsilon^{1/2} \frac{\partial n_d}{\partial \zeta} + \epsilon^{1/2} \frac{\partial n_d u_d}{\partial \zeta} = 0, \quad (2.9)$$

$$\begin{aligned} \epsilon^{3/2} \frac{\partial u_d}{\partial \tau} - V_0 \epsilon^{1/2} \frac{\partial u_d}{\partial \zeta} + \epsilon^{1/2} u_d \frac{\partial u_d}{\partial \zeta} &= \mu \epsilon^{1/2} \frac{\partial \phi}{\partial \zeta} \\ &\quad - \frac{\alpha}{n_d} \frac{\partial n_d}{\partial \zeta} \end{aligned} \quad (2.10)$$

and

$$\begin{aligned} \epsilon^{3/2} \frac{\partial^2 \phi}{\partial \zeta^2} &= \frac{1}{\mu} \left\{ \delta_e \left[ 1 + \sigma_e \phi + \frac{1}{2} \sigma_e^2 \phi^2 + \dots \right] \right. \\ &\quad \left. - \delta_i \left[ 1 - \sigma_i \phi + \frac{1}{2} \sigma_i^2 \phi^2 + \dots \right] + n_d \right\}. \end{aligned} \quad (2.11)$$

We can now expand the variables  $n_d$ ,  $u_d$  and  $\phi$  in the power series of  $\epsilon$ ,

$$\begin{aligned} n_d &= 1 + \epsilon n_d^{(1)} + \epsilon^2 n_d^{(2)} + \dots \\ u_d &= \epsilon u_d^{(1)} + \epsilon^2 u_d^{(2)} + \dots \\ \phi &= \epsilon \phi^{(1)} + \epsilon^2 \phi^{(2)} + \dots \end{aligned} \tag{2.12}$$

Substituting (2.12) into (2.9), (2.10), (2.11) and equating coefficients of  $\epsilon^{3/2}$ , we get, to lowest order,

$$-V_0 \frac{\partial n_d^{(1)}}{\partial \zeta} + \frac{\partial u_d^{(1)}}{\partial \zeta} = 0, \tag{2.13}$$

$$-V_0 \frac{\partial u_d^{(1)}}{\partial \zeta} + \alpha \frac{\partial n_d^{(1)}}{\partial \zeta} - \mu \frac{\partial \phi^{(1)}}{\partial \zeta} = 0 \tag{2.14}$$

and

$$-\frac{h_1}{\mu} \phi - \frac{1}{\mu} n_d^{(1)} = 0. \tag{2.15}$$

After integrating and rearranging terms, the following linear expressions are obtained:

$$u_d^{(1)} = -\frac{\mu V_0}{(V_0^2 - \alpha)} \phi^{(1)}, \tag{2.16}$$

$$n_d^{(1)} = -\frac{\mu}{(V_0^2 - \alpha)} \phi^{(1)} \tag{2.17}$$

and

$$V_0 = \left( \frac{\mu}{h_1} + \alpha \right)^{1/2}, \tag{2.18}$$

where  $h_1 = (T_d \delta_e / T_e + T_d \delta_i / T_i)$  and  $\kappa^2 = \frac{h_1}{\mu} = \frac{a^2}{\lambda_D^2}$ . Equation (2.18) describes how the phase velocity of the DAW changes with  $\alpha$ .

The KdV equation derived for strongly coupled Yukawa fluids using (2.5)–(2.7) and (2.2) is given as

$$\frac{\partial \phi^{(1)}}{\partial \tau} + A \phi^{(1)} \frac{\partial \phi^{(1)}}{\partial \zeta} + B \frac{\partial^3 \phi^{(1)}}{\partial \zeta^3} = 0, \tag{2.19}$$

where the nonlinear coefficient  $A$  and the dispersion coefficient  $B$  are given by

$$A = \left[ \frac{\mu \alpha}{2V_0(V_0^2 - \alpha)} - \frac{3\mu V_0}{2(V_0^2 - \alpha)} + \frac{(V_0^2 - \alpha)h_2}{2V_0 h_1} \right], \tag{2.20}$$

$$B = \frac{(V_0^2 - \alpha)\mu}{2V_0 h_1}, \tag{2.21}$$

with  $h_2 = [\delta_i(T_d/T_i)^2 - \delta_e(T_d/T_e)^2]$ .

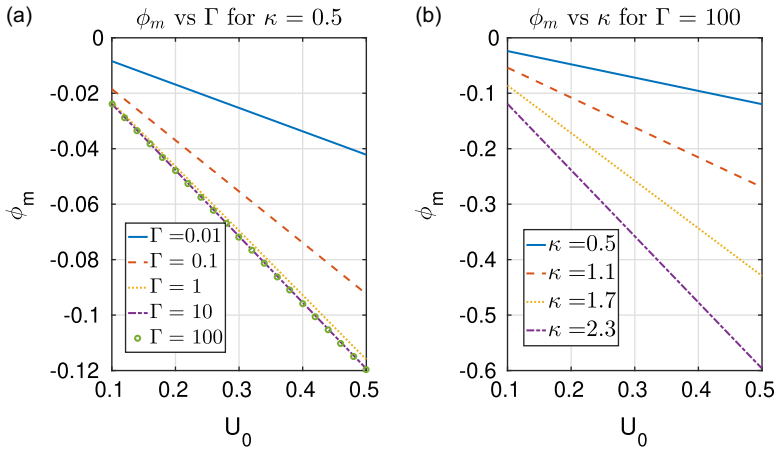


FIGURE 1. The amplitude ( $\phi_m$ ) of the soliton with  $U_0$  is presented in (a) for different values of  $\Gamma$  while keeping  $\kappa = 0.5$ . The amplitude ( $\phi_m$ ) of the soliton with  $U_0$  is presented in (b) for different values of  $\kappa$  while keeping  $\Gamma = 100$ .

Equation (2.19) can be solved by separating variables, resulting in a solution in the laboratory frame,

$$\phi(x, t) = \phi_m \text{sech}^2 \left[ \frac{z}{\Delta} \right], \tag{2.22}$$

where

$$\phi_m = \frac{3U_0}{A} \text{ and } \Delta = \sqrt{\frac{4B}{U_0}}, \tag{2.23}$$

where  $\phi_m$  and  $\Delta$  represent the amplitude and width of the soliton, respectively. Here,  $z$  denotes a coordinate in the laboratory frame, and  $U_0$  is the normalized velocity of the solitary wave.

### 3. Analytical results and their comparison with other approaches

#### 3.1. Analytical KdV solutions using the SFE model

This section presents the variation of the width and amplitude of the solitary structures across a broad range of the  $\Gamma$  and  $\kappa$  parameters. The amplitude  $\phi_m$  and width  $\Delta$  of the solitary structures can be calculated using (2.23). The parameters  $\phi_m$  and  $\Delta$  implicitly depend on  $\Gamma$  and  $\kappa$  through the isothermal compressibility  $\alpha(\Gamma, \kappa)$ , which influences the KdV coefficients  $A$  and  $B$  presented in (2.20) and (2.21), respectively. The variation of the amplitude of the solitary structures is presented in figures 1(a) and 1(b) for different values of  $\Gamma$  and  $\kappa$ , respectively. The value of parameters  $\Gamma$  and  $\kappa$  are considered to characterize the solitary structures in the weak to moderate coupling regime of the system. The variation of  $\phi$  with  $U_0$  for a set of  $\Gamma$  values is presented in figure 1(a), with the value of  $\kappa$  fixed at 0.5. It has been observed that the amplitude increases with  $U_0$  for the fixed values of  $\Gamma$  and  $\kappa = 0.5$ . As can be seen in figure 1(a), the amplitude of the solitary structures also increase with  $\Gamma$  values, however, the increment is more pronounced only at lower values of  $\Gamma$ . In figure 1(a), each colour represents a different value of  $\Gamma$ : blue for  $\Gamma = 0.01$ ; red dotted for  $\Gamma = 0.1$ ; yellow for  $\Gamma = 1.0$ ; purple for  $\Gamma = 10$ ; green circles for  $\Gamma = 100$ . As

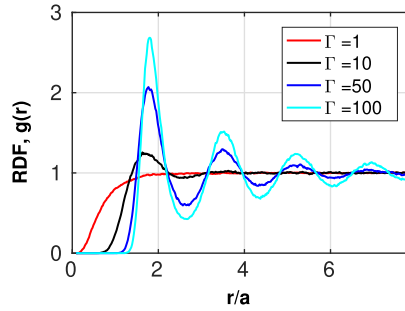


FIGURE 2. The figure illustrates the equilibrium radial distribution function (RDF) various values of the coupling parameter  $\Gamma$ . Peaks in the RDF begin to appear at  $\Gamma \sim 10$  and are most prominent around  $\Gamma \sim 100$ . All results are plotted with a fixed screening parameter of  $\kappa = 0.5$ .

the value of  $\Gamma$  increases, the increment in the amplitude decreases. This dependency is observed up to  $\Gamma = 10$ , beyond which the amplitude remains independent of  $\Gamma$ . It is evident from the overlap of the purple line (for  $\Gamma = 10$ ) and the green circles (for  $\Gamma = 100$ ) in the figure 1(a). It has been observed that the amplitude is highly sensitive to  $\Gamma$  at relatively weak coupling regime and higher values of  $U_0$ . Interestingly, the peak in the RDF start emerging after  $\Gamma > 1$ , as illustrated in figure 2, confirms that the localization of the constituent particles becomes significant for  $\Gamma > 1$ . It can be concluded that the caging of the constituent particles in the potential landscapes does not significantly contribute to the formation of the solitary structures in Yukawa systems. The formation of the solitary structures in this quasilocalized limit will be discussed within the QLCA model further in the upcoming section.

The variation of  $\phi_m$  with  $U_0$  for a set of  $\kappa$  values is presented in figure 1(b), with  $\Gamma$  fixed at 100. It has been observed that the amplitude increases with  $U_0$  for the fixed values of  $\kappa$  and  $\Gamma = 100$ . As depicted in figure 1(b), the amplitude of the solitary structures increases with  $\kappa$  values, and the increment being pronounced across all values of  $\kappa$ . In figure 1(b), each colour represents a different value of  $\kappa$ : blue for  $\kappa = 0.5$ ; red dotted for  $\kappa = 1.1$ ; yellow for  $\kappa = 1.7$ ; purple for  $\kappa = 2.3$ . This occurs because as  $\kappa$  increases, the interaction among particles weakens, making the interaction between neighbouring particles more significant than the collective interactions. We will present a comparison of these observations with the nonlinear QLCA model in the upcoming section.

The variation of  $\Delta$  with  $U_0$  for a set of  $\Gamma$  values is presented in figure 3(a), with  $\kappa$  fixed at 0.5. It has been observed that the width decreases with  $U_0$  for the fixed values of  $\Gamma$  and  $\kappa = 0.5$ . The width of the solitary structures increase with  $\Gamma$  values, however, the increment is more pronounced only at lower values of  $\Gamma$ .

As the value of  $\Gamma$  increases, the increment in the width decreases. This dependency is observed up to  $\Gamma = 10$ , beyond which the width remains independent of  $\Gamma$ . It is evident from the overlap of the purple line (for  $\Gamma = 10$ ) and the green circles (for  $\Gamma = 100$ ) in the figure 3(a). Similar to the cases of amplitude, the width is also highly sensitive to  $\Gamma$  only at relatively weak coupling regime and at higher values of  $U_0$ . The variation of  $\Delta$  with  $U_0$  for a set of  $\kappa$  values is presented in figure 3(b), with  $\Gamma$  fixed at 100. The width decreases with  $\kappa$ , however, the decrement is more pronounced only at lower values of  $\Gamma$ . Solitons are stable, localized wave packets that occur when the nonlinearity, resulting from interactions between dust particles, balances with the dispersion from the collective response of the dusty plasma. As the

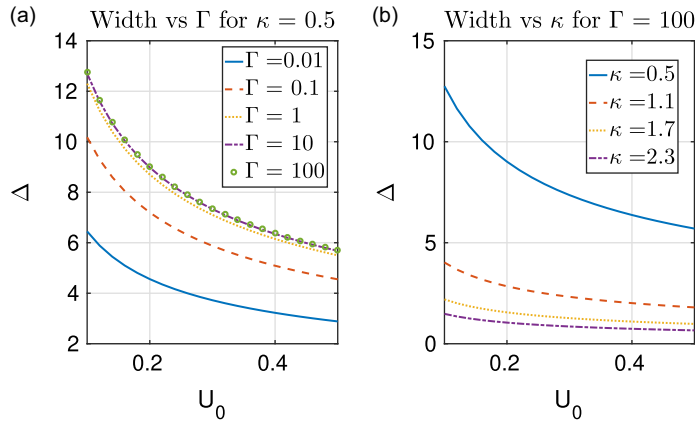


FIGURE 3. The width ( $\Delta$ ) of the soliton with  $U_0$  is presented in (a) for different values of  $\Gamma$  while keeping  $\kappa = 0.5$ . The width ( $\Delta$ ) of the soliton with  $U_0$  is presented in (b) for different values of  $\kappa$  while keeping  $\Gamma = 100$ .

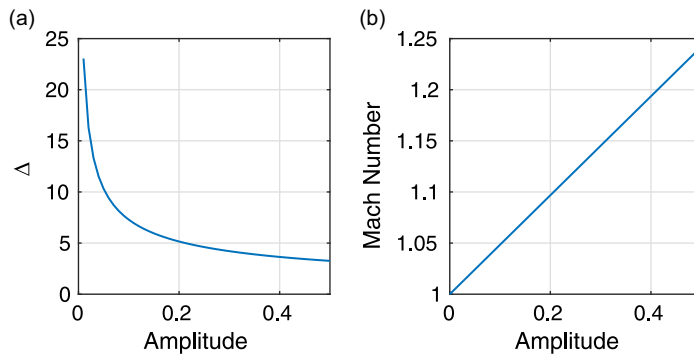


FIGURE 4. The width and Mach number are plotted with the soliton amplitude in (a) and (b), respectively, for  $\kappa = 0.3$  and  $\Gamma = 100$ .

dust temperature increases, or equivalently as the coupling parameter  $\Gamma$  decreases, this balance is disrupted because the effects of nonlinearity weaken. This disruption leads to the formation of broader and shorter solitons.

### 3.2. Experimental validations of the SFE model

This section is dedicated to providing experimental validation of the SFE model. The variation of the Mach number and the width  $\Delta$  of the soliton structures for the normalized amplitude is presented in figure 4 under the same experimental conditions (Sharma, Boruah & Bailung, 2014). The width of the soliton presented in figure 4(a) decreases with the normalized amplitude of the soliton. The Mach number presented in figure 4(b) increases with the normalized amplitude of the soliton. These analytical results show a good quantitative agreement with the experimentally measured values of the width and the Mach number with normalized amplitude (see Sharma, Boruah & Bailung, 2014). Agreement is achieved for lower values of  $\kappa$ ,

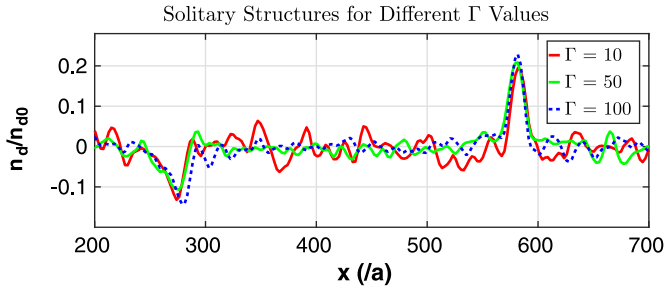


FIGURE 5. The snapshot of the solitary waves at time, induced by an electric field perturbation with a magnitude of  $E = 25.40$ , for different values of  $\Gamma$ . The solitary pulse, depicted in red and green and blue dotted, emerges at  $\Gamma = 10$ ,  $\Gamma = 50$  and  $\Gamma = 100$ , respectively, with a fixed screening parameter of  $\kappa = 0.5$ .

and the characteristics of the soliton are not significantly altered by varying the  $\Gamma$  parameter.

### 3.3. Validations with MD simulations

In this section, the MD simulations are conducted to validate the theoretically predicted results across a range of  $\Gamma$  values. The soliton structures shown in figure 5 are excited by applying an electric field within a small region of the rectangular simulation box. Further details regarding the simulation parameters and methodology can be referenced in our previous work (Prince Kumar and Devendra Sharma, 2024). Figure 5 represents the soliton-like structures for the various values of  $\Gamma$  and a constant  $\kappa = 0.5$ . The red, green and dotted blue lines represent the soliton profiles for  $\Gamma = 10$ , 50 and 100, respectively. It can be seen from figure 5 that the characteristic properties of the solitons remain independent of  $\Gamma$ . These results are in close quantitative agreement with the theoretical predictions shown in figures 1 and 3. They predict that the amplitude and width of the solitons remain independent of  $\Gamma$  beyond  $\Gamma \sim 10$  (the onset of localization). Therefore, the theoretical model accurately predicts the onset of localization and its effects on the nonlinear excitations in Yukawa media.

### 3.4. Comparison with the nonlinear QLCA model

In this section, we present a brief comparison between the SFE model and the nonlinear QLCA model across various sets of  $\Gamma$  and  $\kappa$  parameters. The basic equations for the nonlinear QLCA model are presented in appendix B. The QLCA model, due to its construction, remains applicable to the highly localized regime, whereas the SFE model also tends to cover a relatively weak coupling regime. The fluid model's limited scope prevents it from accessing relatively shorter collective modes, as its phenomenological equation of state is not applicable in this limit. The contribution of relatively shorter wavelengths to the formation of soliton structures becomes significant in the stronger screening limit ( $\kappa > 1$ ), a phenomenon successfully described by the nonlinear QLCA model. Figure 6 illustrates the solitons derived from the simple fluid and the nonlinear QLCA model for various values of  $\kappa$ . The results plotted for  $\kappa = 0.3$  and 1.0 in figure 6(a) and 6(b), respectively, show that the SFE model agrees with the observations of the nonlinear QLCA model in the weak screening

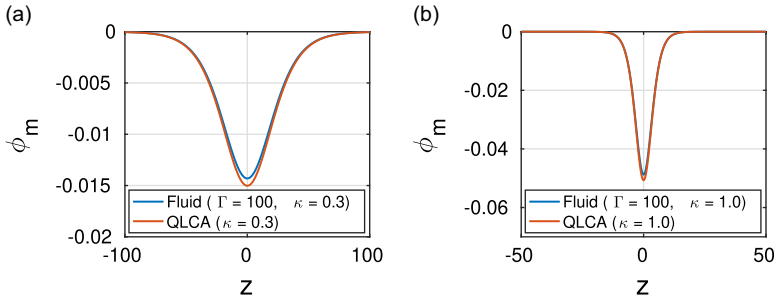


FIGURE 6. The soliton profiles calculated from the SFE model and QLCA for  $\kappa = 0.3$  and  $\kappa = 1.0$  are presented in (a) and (b), respectively. The value of the parameter  $\Gamma$  is considered to remain within the quasilocalized regime of the medium.

limit. The soliton structures are derived within the nonlinear QLCA framework utilizing the analytical form of the D-matrix, which is calculated using the isothermal compressibility as outlined in (B.4). However, the description of the relatively high screening regime of nonlinear excitations requires a more sophisticated form of the D-matrix capable of accommodating the relatively higher modes in the formulation. Moreover, the significance contribution to the formation of the KdV solitons comes from lower spectral modes that are efficiently captured within the framework of the SFE model. The QLCA results confirm the applicability of the SFE model in describing the weak to moderate screening regime of the solitons in Yukawa media.

### 3.5. Comparison with the GH model

In this section, we present a brief comparison between the SFE model and the GH model for describing the solitons in Yukawa media. A brief introduction to the KdV equations derived within the GH framework is provided in appendix C. The KdV coefficients are the function of the system excess energy via the relaxation time ( $\tau_m$ ) and the coefficient of viscosity ( $\eta$ ). Since the excess energy  $u(\Gamma)$  of the medium remains independent of  $\kappa$ , this version of the model has a limited scope, preventing it from effectively exploring the wide range of the screening regime of the nonlinear excitations in Yukawa media. However, the SFE model has accessibility to explore the relatively high screening regime of the solitons in Yukawa fluids, as the internal energy and the compressibility in the model are the explicit functions of the  $\kappa$  (see (A.1) and (A.5)). The Mach number and the width  $\Delta$  of the soliton structures for the normalized amplitude are depicted in figure 4. These results can also be reproduced using the GH model for a specific set of experimental parameters (Sharma, Boruah & Bailung, 2014). These observations further confirm the efficacy of the SFE model in describing the nonlinear excitations in strongly coupled Yukawa systems. Similar to the case of the SFE model, we also observe from the GH model that the characteristics of the soliton structures do not depend on the  $\Gamma$  value. However, the GH model proves more accurate in describing the effects of shear waves in the medium, an area where the SFE model falls short.

### 3.6. Numerical simulations with the general perturbations

To simulate the evolution of the general perturbations governed by (2.5)–(2.7) and (2.2), we employ a pseudospectral technique utilizing the fast Fourier transform

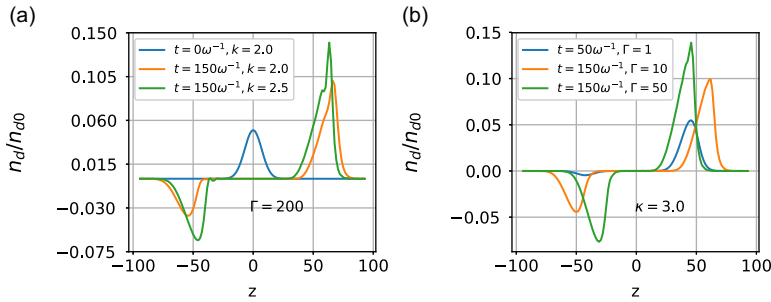


FIGURE 7. The figure illustrates the progression of an initial gaussian density perturbation characterized by a width  $\Delta = 10$  and an amplitude  $A = 0.05$ . Panels (a) and (b) correspond to different values of  $\kappa$  and  $\Gamma$ , respectively.

library (Frigo, May 1999). These discretization schemes are chosen to adhere to the Courant–Friedrichs–Lewy condition (Russell, 1989). For time integration, we employ the Adams–Bashforth method (Durrant, 1991). The aliasing effects induced by nonlinear terms are mitigated using the well-established two-thirds rule proposed by Orszag (Patterson & Orszag 1971). We apply an initial Gaussian pulse in the medium for a wide range of  $\Gamma$  and  $\kappa$  values. The mathematical form of the profile is written as

$$n_d = n_0 \exp \left[ - \left( \frac{z - z_0}{\Delta} \right)^2 \right], \tag{3.1}$$

where  $\Delta$  and  $n_0$  are the width and amplitude of the perturbation. The initial density perturbation, depicted in figure 7(a) with a blue colour for  $\kappa = 2.0$ , disintegrates into positive and negative density profiles travelling in opposite directions. The snapshot of the profile at  $t\omega_{pd} = 150$  is shown in yellow in figure 7(b). To investigate the effects of  $\kappa$ , we further evolve the initial perturbation with  $\kappa = 2.5$  and present the snapshot of the density at  $t = 150\omega_{pd}$  in figure 7(a) with the green colour. The increment in the intensity of the refractive soliton with  $\kappa$  is also confirmed with the MD simulation results (Donkó *et al.* 2020). Now, we are interested in exploring the effects of  $\Gamma$  on the evolution of the general density perturbations. Therefore, the snapshot of the disintegrated profiles is plotted in figure 7(b) for different values of  $\Gamma$ . The blue, red and green colours represent the profile at  $t = 50\omega_{pd}^{-1}$  for  $\Gamma = 1.0$ ,  $t = 50\omega_{pd}^{-1}$  for  $\Gamma = 10$  and  $t = 50\omega_{pd}^{-1}$  for  $\Gamma = 50$ , respectively. This shows that the intensity of rarefactive solitons decreases with  $\Gamma$ , and no rarefactive solitons are observed beyond  $\Gamma = 1$  at  $\kappa = 3.0$ .

#### 4. Summary and conclusions

We have introduced the SFE model to describe the nonlinear excitations in strongly coupled Yukawa fluids across a broad spectrum of  $\Gamma$  and  $\kappa$  values. The equation of state of the medium is obtained using the practical expressions for the internal energy and pressure, which are applicable across a wide range of the coupling regime. The formulation describes the solitons across a wide spectrum of parameters  $\Gamma$  and  $\kappa$  values, encompassing the respective domains of applicability of the nonlinear QLCA and GH models in characterizing the solitons in Yukawa media. The formulation also reproduces the experimentally measured values of the

width and Mach number for various values of the normalized amplitude (Sharma, Boruah & Bailung, 2014). It has been observed that the amplitude and width of the soliton in weak coupling limit (no-localization) increases with  $\Gamma$  up to the value  $\Gamma \sim 10$ , beyond this value it remains independent to  $\Gamma$  values. The MD simulations confirm that the localization starts emerging beyond  $\Gamma \sim 10$  which shows not impact on the solitons in Yukawa media.

The SFE model may successfully overcome the limitations of the nonlinear QLCA in the weak coupling regime and the one component plasma version GH model in the strong screening limit of solitons in Yukawa media. It is known that the simplistic fluid treatment (Prince Kumar and Devendra Sharma, 2020) is applicable to longer wavelengths or low frequencies and becomes irrelevant in the highly localized regime. The fluid model's limited scope prevents it from accessing relatively shorter collective modes, as its phenomenological equation of state is not applicable in this limit. However, the significant contribution to the formation of the KdV solitons comes from lower spectral modes, which are efficiently captured within the framework of the SFE model. Additionally, the precise practical formulations of thermodynamic quantities enable us to achieve quantitative results and conduct detailed comparisons with outcomes from other approaches. The SFE model presents a distinctive opportunity to precisely quantify the longitudinal nonlinear excitations and their instabilities of Yukawa or dusty plasma systems (Sandip Dalui, Prince Kumar, and Devendra Sharma, 2023). This is facilitated by the explicit dependency of the compressibility, pressure, adiabatic index and internal energy of the system on  $\Gamma$  and  $\kappa$ . One of the example is modulational instability which is likely to occur in frequency ranges where the dispersion relation of the DAW exhibits anomalous behaviour, such as regions of negative dispersion. In a specific range of  $\Gamma$  and  $\kappa$ , the compressibility changes its sign to negative, resulting in a negative dispersion relation at a certain  $k$  value. As a consequence, the group velocity approaches zero at a specific value of  $k$  and subsequently becomes negative. In this context, it would be interesting to investigate how variations in  $\Gamma$  and  $\kappa$  influence the modulational instability of the dust acoustic modes.

The present work can be of finite interest to the complex (dusty) plasma and nonlinear plasma waves communities. It offers valuable insights into the underlying physics of nonlinear excitations, which can significantly benefit researchers in this field. This is achieved through its construction, which includes explicit expressions for thermodynamic quantities that account for both particle–particle correlations and plasma-related effects. For example, while the adiabatic index  $\gamma$  shows a discontinuity at moderate coupling (Khrapak & Thomas 2015), this does not impact the dust solitary structures. The structures are governed by the product  $\gamma\alpha$ , which remains finite, as compressibility vanishes in this regime. A more specific analysis will be conducted in future work.

### Acknowledgements

The simulations are performed on the Antya cluster at the Institute for Plasma Research (IPR).

*Editor Edward Thomas, Jr. thanks the referees for their advice in evaluating this article.*

### Declaration of interests

The authors report no conflict of interest.

**Appendix A. Thermodynamic functions for strongly coupled Yukawa systems**

The main objective is to calculate the isothermal compressibility  $\alpha$  of a strongly coupled Yukawa medium. The practical expressions of the thermodynamic quantities for strongly coupled Yukawa systems has been derived using the ion spherical model assumptions Khrapak *et al.* (2014). The expression for the internal energy parameter is written as

$$u(\kappa, \Gamma) = \frac{3}{2} + \epsilon + \left[ \frac{\kappa(\kappa + 1)\Gamma}{(\kappa + 1) + (\kappa - 1)e^{2\kappa}} \right] + \delta \left( \frac{\Gamma}{\Gamma_m} \right)^{2/5} - \frac{3\Gamma}{2\kappa^2} - \frac{\kappa\Gamma}{2}, \tag{A.1}$$

where the last two terms correspond to the plasma-related contribution to the internal energy of the medium. The explicit expression for the compressibility factor is given as Khrapak & Thomas (2015)

$$Z(\kappa, \Gamma) = \left( 1 + \frac{\epsilon}{3} \right) + \frac{\Gamma\kappa^4}{6[\kappa \cosh(\kappa) - \sinh(\kappa)]^2} + \frac{\delta}{3} \left( \frac{\Gamma}{\Gamma_m} \right)^{2/5} f_Z(\beta\kappa), \tag{A.2}$$

where

$$f_Z(x) = \frac{x^3 + x^2 + 2x + 2}{x^2 + 2x + 2}. \tag{A.3}$$

The isothermal compressibility modulus is related to the compressibility factor via

$$\alpha = Z + \frac{\Gamma}{3} \frac{\partial Z}{\partial \Gamma} - \frac{\kappa}{3} \frac{\partial Z}{\partial \kappa}. \tag{A.4}$$

This yields

$$\alpha(\kappa, \Gamma) = \left( 1 + \frac{\epsilon}{3} \right) + \frac{\Gamma\kappa^6 \sinh(\kappa)}{9[\kappa \cosh(\kappa) - \sinh(\kappa)]^3} + \frac{\delta}{45} \left( \frac{\Gamma}{\Gamma_m} \right)^{2/5} f_\alpha(\beta\kappa), \tag{A.5}$$

where

$$f_\alpha(x) = \frac{2x^6 + 14x^5 + 35x^4 + 76x^3 + 136x^2 + 136x + 68}{(x^2 + 2x + 2)^2}. \tag{A.6}$$

The pressure of the medium can be expressed in term of the compressibility factor  $Z(\kappa, \Gamma)$  as,  $p(\kappa, \Gamma) = Z(\kappa, \Gamma) + (3\Gamma/2\kappa^2 - 1)$ . The coupling parameter at fluid–solid phase transition is  $\Gamma_m \sim \left[ 172 \exp(\beta\kappa) / \left( 1 + \beta\kappa + \frac{1}{2}\beta^2\kappa^2 \right) \right]$ , and the value of parameters  $\epsilon = -0.1$ ,  $\beta = 1.614$  and  $\delta = 3.2$  are considered for the present analysis.

**Appendix B. The nonlinear QLCA model for Yukawa fluids**

The momentum conservation equation retaining localizations via QLCA basis is given as Prince Kumar and Devendra Sharma (2023)

$$\frac{\partial u_{dx}}{\partial t} + u_{dx} \frac{\partial u_{dx}}{\partial x} = \mu \frac{\partial \phi}{\partial x} - \tilde{\alpha} \frac{1}{n_{dx}} \frac{\partial n_{dx}}{\partial x}, \tag{B.1}$$

which is supplemented by the continuity

$$\frac{\partial n_{dx}}{\partial t} + \frac{\partial}{\partial x}(n_{dx}u_{dx}) = 0, \quad (\text{B.2})$$

and the Poisson equation

$$\frac{\partial^2 \phi}{\partial x^2} = \frac{1}{\mu} [n_d + n_e - n_i], \quad (\text{B.3})$$

respectively. Equations (B.1)–(B.3) form a nonlinear QLCA model. The analytical form of the isothermal compressibility factor within the QLCA basis is given by

$$\alpha(\kappa) = -0.0799 - 0.0046\kappa^2 + 0.0016\kappa^4 \quad (\text{B.4})$$

Furthermore, a more sophisticated form of the D-matrix can be incorporated via a pseudospectral technique, as discussed in Prince Kumar and Devendra Sharma (2023)

### Appendix C. The KdV equation from the GH model

The GH model was adopted by the dusty plasma community to study the effects of the viscoelastic nature of the medium on its collective excitations. The viscoelastic contribution incorporated via the relaxation time ( $\tau_m$ ) shows the finite effects on the linear and collective excitations of the medium. The details about the model equations can be found in Kaw & Sen (1998). As a particular interest here to analysis the KdV equations derive within the framework of the GH model, can be written as Sharma, Boruah & Bailung (2014)

$$\frac{\partial n^{(1)}}{\partial \tau} + An^{(1)} \frac{\partial n^{(1)}}{\partial \zeta} + B \frac{\partial^3 n^{(1)}}{\partial \zeta^3} = 0, \quad (\text{C.1})$$

where the nonlinear coefficient  $A$  and the dispersion coefficient  $B$  are given by

$$A = \frac{2\alpha\lambda + [\beta(\mu_e\sigma_e^2 - \mu_i)\lambda/\beta^2] - \lambda^3\tau_m}{(\alpha - 2\lambda^2\tau_m + \tau_m)}, \quad (\text{C.2})$$

$$B = \frac{\alpha\lambda}{(\alpha - 2\lambda^2\tau_m + \tau_m)}, \quad (\text{C.3})$$

where  $\alpha = \eta^* - \lambda^2\tau_m$ ,  $\beta = \mu_e\sigma_e + \mu_i$ . The parameter  $\eta^*$  is the viscosity coefficient whose empirical analytical expression can be written as  $\eta = a(\Gamma_m/\Gamma) + b(\Gamma/\Gamma_m) + c$ , where the table for the unknown coefficients is given in Saigo & Hamaguchi (2002). The memory relation time  $\tau_m = 3\eta^*\Gamma[1 - \gamma\mu + 0.266u(\Gamma)]^{-1}$  follows the trend of the viscosity parameter  $\eta^*$  Chakrabarti & Ghosh (2015). The compressibility  $\mu$  is calculated from the excess energy for one component plasma ( $\kappa = 0$ ) for the range  $1 < \Gamma < 200$ . Therefore, the scope of the presented form of the GH model is limited in describing the relative strong screening regime of the medium.

### REFERENCES

- ARORA, G., RANI, R. & EMADIFAR, H. 2022 Soliton: a dispersion-less solution with existence and its types. *Helvion* **8** (12), e12122.

- CHAKRABARTI, N. & GHOSH, S. 2015 Longitudinal dust acoustic solitary waves in a strongly coupled complex (dusty) plasma. *J. Plasma Phys* **81** (3), 905810310.
- CHAMON, C. 2000 Solitons in carbon nanotubes. *Phys. Rev. B* **62** (4), 2806–2812.
- CRAIG, W., GUYENNE, P., HAMMACK, J., HENDERSON, D. & SULEM, C. 2006 Solitary water wave interactions. *Phys. Fluids* **18** (5), 057106.
- DAVIDSON, R. 2012 *Methods in Nonlinear Plasma Theory*. Elsevier.
- DONKÓ, Z., HARTMANN, P., MASHEYEVA, R. U. & DZHUMAGULOVA, K. N. 2020 Molecular dynamics investigation of soliton propagation in a two-dimensional yukawa liquid. *Contrib. Plasm. Phys.* **60** (8), e201900197.
- DURRAN, D. R. 1991 The third-order adams-bashforth method: an attractive alternative to leapfrog time differencing. *Mon. Weather Rev.* **119** (3), 702–720.
- FRIGO, M. MAY. 1999 A fast fourier transform compiler. *SIGPLAN Not* **34** (5), 169–180.
- GOLDEN, K. I. & KALMAN, G. J. 2000 Quasilocalized charge approximation in strongly coupled plasma physics. *Phys. Plasmas* **7** (1), 14–32.
- GORDON, J. 1983 Interaction forces among solitons in optical fibers. *Opt. Lett* **8** (11), 596–598.
- GU, C. 2013 *Soliton Theory and Its Applications*. Springer Science & Business Media.
- KAW, P. 2001 Collective modes in a strongly coupled dusty plasma. *Phys. Plasmas* **8** (5), 1870–1878.
- KAW, P. & SEN, A. 1998 Low frequency modes in strongly coupled dusty plasmas. *Phys. Plasmas* **5** (10), 3552–3559.
- KHRAPAK, S., KHRAPAK, A., IVLEV, A. & THOMAS, H. 2014 Ion sphere model for yukawa systems (dusty plasmas). *Phys. Plasmas* **21** (12), 123705.
- KHRAPAK, S. A. & THOMAS, H. M. 2015 Fluid approach to evaluate sound velocity in yukawa systems and complex plasmas. *Phys. Rev. E* **91** (3), 033110.
- KHRAPAK, S. A. & THOMAS, H. M. 2015 Practical expressions for the internal energy and pressure of yukawa fluids. *Phys. Rev. E* **91** (2), 023108.
- KUMAR, S., TIWARI, S. K. & DAS, A. 2017 Observation of the korteweg-de vries soliton in molecular dynamics simulations of a dusty plasma medium. *Phys. Plasmas* **24** (3), 033711.
- KUMAR, S., VIJ, S., KANT, N. & THAKUR, V. 2022 Resonant terahertz generation by the interaction of laser beams with magnetized anharmonic carbon nanotube array. *Plasmonics* **17** (4), 381–388.
- PATTERSON, G. & ORSZAG, S. A. 1971 Spectral calculations of isotropic turbulence: efficient removal of aliasing interactions. *Phys. Fluids* **14** (11), 2538–2541.
- PRINCE KUMAR and DEVENDRA SHARMA. 2020 Dust vortex flow analysis in weakly magnetized plasma. *Phys. Plasmas* **27** (6), 063703.
- PRINCE KUMAR and DEVENDRA SHARMA. 2021 Collective excitations of rotating dusty plasma under quasi-localized charge approximation of strongly coupled systems. *Phys. Plasmas* **28** (8), 083704.
- PRINCE KUMAR and DEVENDRA SHARMA. 2022 Quasi-localized charge approximation (qlca) approach for the nonlinear structures in strongly coupled yukawa systems, (APS Division of Plasma Physics Meeting Abstracts, pages BO07–015, **2022**
- PRINCE KUMAR and DEVENDRA SHARMA. 2023 Quasi-localized charge approximation approach for the nonlinear structures in strongly coupled yukawa systems. *Phys. Plasmas* **30** (3), 033702.
- PRINCE KUMAR and DEVENDRA SHARMA. 2024 Numerical validation of yukawa fluid excitations within the quasilocalized charge approximation (qlca) theory. *Contrib. Plasm. Phys.* **64** (6), e202400026.
- RUSSELL, T. 1989 Stability analysis and switching criteria for adaptive implicit methods based on the cfl condition, (SPE Reservoir Simulation Conference, pages SPE–18416, SPE.
- SAIGO, T. & HAMAGUCHI, S. 2002 Shear viscosity of strongly coupled yukawa systems. *Phys. Plasmas* **9** (4), 1210–1216.
- SANDIP DALUI, PRINCE KUMAR, and DEVENDRA SHARMA. 2023 Modulational instability of a yukawa fluid excitation under the quasi-localized charged approximation (qlca) framework. *Phys. Scripta* **98** (2), 025606.
- SHARMA, S., BORUAH, A. & BAILUNG, H. 2014 Head-on collision of dust-acoustic solitons in a strongly coupled dusty plasma. *Phys. Rev. E* **89** (1), 013110.
- SHUKLA, P. 1983 *Solitons in Plasma Physics*. Cambridge University Press, page197–220.
- TIWARI, S. K., DAS, A., SEN, A. & KAW, P. 2015 Molecular dynamics simulations of soliton-like structures in a dusty plasma medium. *Phys. Plasmas* **22** (3), 033706.